In-flight temperature and velocity of powder particles of plasma-sprayed TiO2

Cizek, Jan; Khor, Khiam Aik; Dlouhy, Ivo

2013

Cizek, J., Khor, K. A., & Dlouhy, I. (2013). In-Flight Temperature and Velocity of Powder Particles of Plasma-Sprayed TiO2. Journal of Thermal Spray Technology, 22(8), 1320-1327.

https://hdl.handle.net/10356/103646

https://doi.org/10.1007/s11666-013-9993-9

JTTEE5
DOI: 10.1007/s11666-013-9993-9
1059-9630/$19.00 © ASM International

In-Flight Temperature and Velocity of Powder Particles of Plasma-Sprayed TiO_2

Jan Cizek, Khiam Aik Khor, and Ivo Dlouhy

(Submitted April 10, 2013; in revised form August 20, 2013)

This paper relates to the in-flight temperature and velocity of TiO_2 particles, an integral part of the systematic research on atmospheric plasma spraying of the material. Initial powder feedstock (32-45 μm, 100% rutile phase) was introduced into the plasma jet. Six parameters were selected to represent the versatility of the plasma system and their respective influences were determined according to basic one-at-a-time and advanced Taguchi design of experiments combined with the analysis of variance analytical tool. It was found that the measured temperatures varied from 2121 to 2830 K (33% variation), while the velocities of the particles were altered from 127 to 243 m/s (91% variation). Gun net power was detected as the most influential factor with respect to the velocity of the TiO_2 particles (an increase of 8.4 m/s per 1-kW increase in net power). Spray distance was determined to have a major impact on the in-flight temperature (a decrease of 10 mm in spray distance corresponds to a drop of 36 K). A significant decrease in both characteristics was detected for an increasing amount of powder entering the plasma jet: A drop of 7.1 K and 1.4 m/s was recorded per every +1 g/min of TiO_2 powder.

Keywords in-flight properties, plasma spray, rutile, Taguchi design, TiO_2, titania

1. Introduction

The selection of bio-materials used in present in vivo applications has grown considerably in the last few decades. Due to the prospective contact with biological tissues, the potential material candidates have to exhibit at least bio-tolerable levels of compatibility at the interface. The final selection of the most suitable bio-material (or a combination of materials) for a specific application is influenced by design requirements (function, objectives, constraints), anticipated loading (expected service life, mechanical loading, environmental impact), and also its availability and cost.

Generally, the inherent physical, chemical, and (in the case of, e.g., load-bearing applications) mechanical properties of the materials are considered as the primary factors. In some cases, materials selected for their favorable physical properties but that do not meet the required stringent bio-requirements have to be shielded (in case of, e.g., hard tissue implants) by modifications of their respective surfaces (Ref 1). Aside from the traditionally applied bone-resembling ceramics (e.g., various calcium phosphates, hydroxyapatite), experimental efforts are carried out for utilization of novel materials for the shielding applications. One such material is TiO_2.

Of the three polymorphs of titania (brookite, rutile, anatase), the biocompatible properties of the latter two modifications have been noted in the literature (improved hemocompatibility as well as biocompatibility) (Ref 2, 3). Anatase coatings were proven to enhance implant osseointegration in vivo (cell adhesion, spreading, proliferation, and differentiation) and influence expression of various genes in cultured osteoblast-like cell lines (Ref 4). Rutile layers were proven to decrease the levels of bioreactivity of titanium implants in human osteoblast cultures and improve their biocompatibility without compromising the cell viability (Ref 5). Both polymorphs were proven to enhance the osteoblast compatibility of PEEK material in terms of cell adhesion, cell proliferation, and differentiation abilities and osteogenesis performance (Ref 6). Further to that, it was shown that the rutile phase is more stable than the anatase phase at low and high pH (Ref 7) and that a change in a structure from anatase to rutile resulted in a substantial decrease of the dissolution rate of metallic ions in a simulated body fluid (Ref 8).

Various methods are commonly used for deposition of TiO_2 layers onto function-performing core materials. Due to the typical high temperatures achieved in the process (and, therefore, the versatile ability to process a majority of known materials incl. oxides), plasma spraying is employed frequently (Ref 9). Plasma spraying is a line-of-sight technology process utilized for deposition of various materials onto (usually mechanically, thermally, or

This article is an invited paper selected from presentations at the 5th Asian Thermal Spray Conference (ATSC 2012) and has been expanded from the original presentation. ATSC 2012 was held at the Tsukuba International Congress Center, Ibaraki, Japan, November 26-28, 2012, and was organized by the Japan Thermal Spray Society and the Asian Thermal Spray Society.

Jan Cizek and **Ivo Dlouhy**, Institute of Materials Science and Engineering, NETME Centre, Brno University of Technology, Brno, Czech Republic; and **Khiam Aik Khor**, School of Mechanical and Aerospace Engineering, Nanyang Technological University, Singapore, Singapore. Contact e-mail: cizek@fme.vutbr.cz.

Published online: 14 September 2013

chemically altered) substrates. The sprayed material is fed into the plasma jet generally in a form of powder with particle sizes determined by the particular requirements (generally 5-100 μm). Upon entering the plasma jet, the powder particles are swept away by the flux of ionized gases and accelerated toward the substrate. Simultaneously, the temperature of the particles increases due to heat intake from the plasma flux and eventually reaches a melting point of the selected material. As the plasma torch moves over the substrate, the heated, semi- or fully molten particles impinge on the surface, undergo morphological changes to conform to the underlying layers, and solidify, creating so-called splats (Ref 10). Successive passes of the plasma torch result in stacking up of the material and build-up of the coating. Consisting of solidified splats, impurities and inclusions, oxide particles, voids, and porosity, the produced coating has a heterogeneous, anisotropic structure (Ref 9). Further to that, the solid → liquid → solid transition frequently induces changes of the feedstock material, in particular phase changes (e.g., rutile ↔ anatase).

Apart from the initial material feedstock properties, the trajectory of the particles within the plasma jet and their respective in-flight temperatures and velocities are the crucial factors having effects on the final coatings properties. Controlling the two factors is therefore essential for the prospective successful application of coated implants. As these factors are directly linked to the plasma system parameters (including the spray distance factor), the influence of six selected plasma spray system factors on the in-flight properties of the TiO_2 particles has been studied in the presented work.

2. Experimental Setup

2.1 Powder Feedstock

A commercially available TiO_2 powder (HC Starck, Germany) was purchased at the initial particle sieve range of 18-46 μm. As the in-flight properties that the individual particles acquire in the plasma jet (e.g., velocities, level of melting) are significantly influenced by the respective particle's mass (and, therefore, its diameter), a sieving procedure was employed to lessen the prospective variances. For the subsequent experimental work, only the 32-45 μm fraction was used. No ≤ 3-μm dust was detected in the powder as measured by the laser scattering method (Fritsch Analysette NanoTec22).

The angular morphology of the powder was observed in SEM (a consequence of the fused and crushed production route, Fig. 1a). Despite its morphology, the powder exhibited good flowability. Cross-sectional analysis of the powder revealed the inherent internal porosity of the material (Fig. 1b). Due to the low detection threshold of the software image analysis, the levels of the internal porosity of the TiO_2 powder were specified by a helium pycnometry method (13.62%).

The chemical composition of the powder as provided by the manufacturer could be seen from Table 1. In order to ascertain the relative content of the two most common TiO_2 polymorphs (rutile and anatase, both tetragonal) in the feedstock, Rietveld analysis of the obtained XRD spectrum was carried out (4.0% content of anatase phase). In order to induce phase transformations so as to obtain the maximum proportion of the (more stable) rutile phase, heat treatment of the feedstock was carried out at 1270 K for 240 min (some of the measured internal porosity content might have originated from the anatase → rutile transformation) (Ref 11). The effect of the heat treatment was confirmed by a subsequent XRD analysis as the powder was measured as 100% rutile (Fig. 2, PowderCell software prediction of a rutile phase pattern provided for reference). The impurities indicated by the manufacturer (hematite, quartz) or traces of brookite (orthorhombic TiO_2 phase) were not detected in the spectrum.

2.2 Plasma System

Atmospheric plasma system (Praxair Inc., USA, SG-100 internal-injection gun) was used in the experiment. Argon was used as the powder-carrying gas and a mixture of argon and helium was used as the arc-forming gas. Six

Table 1 Indicated chemical composition of TiO_2 powder

Compound	Mass fraction, %
TiO_2	Balance
Fe_2O_3	0.25
SiO_2	0.30

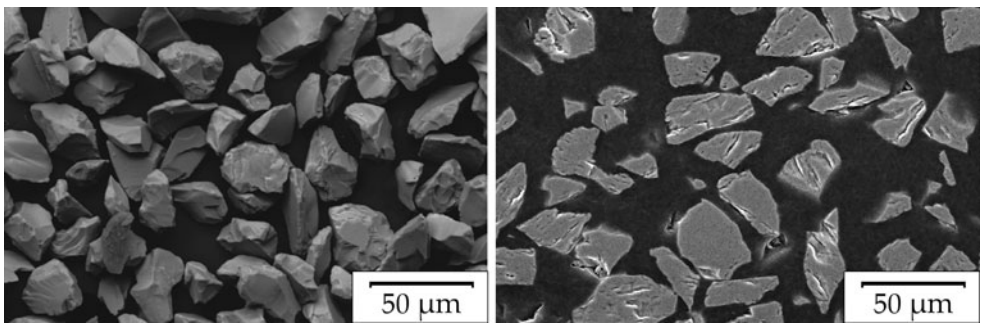

Fig. 1 Morphology and cross section of TiO_2 powder

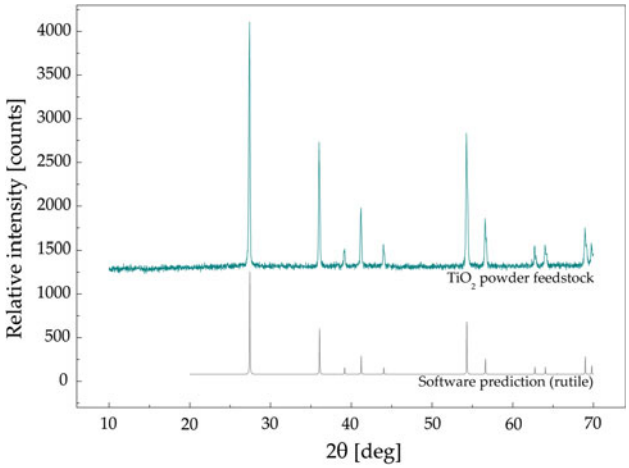

Fig. 2 Measured XRD spectrum of TiO_2 powder feedstock, observable peaks pertain to rutile phase

parameters were selected to represent the versatility of the system: net power, flow of the main (Ar) and auxiliary (He) gases, powder feed rate, flow of the carrier gas (Ar), and spray distance, i.e., the distance between the gun and the target. The six factors represent the most robust parameters influencing the properties of the generated jet and therefore the in-flight properties the powder particles attain. Description of the individual factors could be found, e.g., in the study (Ref 12). The feed rate factor (amount of powder entering the jet per minute) was quantified by an additional powder-collecting experiment at various powder feeder wheel revolutions (1-4 rpm).

Preliminary experiments on the stability of the used plasma system showed a high stability considering the characteristics of the generated plasma jet. The maximum variations of the in-flight properties were specified as 1% for temperature and 3% for velocity for multiple (5×) plasma jet ignitions under identical parameters levels.

2.3 In-Flight Properties

2.3.1 In-Flight Measurement Tools. In order to detect the TiO_2 particles during their dwell time in the plasma jet and to quantify their respective selected in-flight properties (e.g., temperature, velocity, flux, divergence), a fast-shutter CCD camera system (SprayWatch, Oseir Ltd., Finland) was employed. The camera detection capabilities were enhanced by an attached laser-beam illumination system (Hi-Watch, 808 ± 5 nm wavelength). The positioning of the detection devices (camera lens and laser emission axis) was perpendicular with respect to the plasma jet axis (orthogonal setup). In order to detect the entire volume of the plasma jet at various spray distances, the focal distance of the camera (lens to jet axis) was set to 235 mm. In order to maintain the mutual comparability of the results, manual configuration of the camera (exposure time of 15 μs, aperture 80%) was used for all measurements and the respective data were collected for at least 1 min for each run. An average of the measured in-flight properties from two system runs was calculated in all measurements to further increase the results' reliability.

2.3.2 One-at-a-Time Method. In the first part, the influence of the six selected factors on the in-flight properties was measured based on a full-factorial design of experiment ("several parameters, one-at-a-time," "OAAT" (Ref 13)). In this setup, the values of the observed parameter are changed by a pre-defined step over a selected range, while the other parameters are kept at constant values (method layout provided in Table 2). The interval limits of the individual parameters were selected to span the typical working ranges of the SG-100 equipped plasma system. The major advantage of the OAAT setup is its accurate determination of the respective parameter's effect. However, the method is resource and time consuming and does not allow the integration of the parameters' mutual interaction.

2.3.3 Taguchi Design of Experiment. In order to involve the potential interactions, the full-factorial design was supplemented by Taguchi design of experiment (Ref 14). Its statistical-based concept effectively combines the individual factor levels, resulting in high efficiency of the experimental design, while maintaining the primary information yield. By conducting the experimental work according to this partial-factorial setup, the number of necessary measurements was substantially reduced (from $3^6 = 729$ to 18 for six three-level factors). Given the number of factors, their respective number of levels (three), involvement of the mutual bonds, and the reliability and repeatability of the results, the layout of a corresponding orthogonal array (L-18) could not be used in its standardized form for the experiments. Following the procedure provided in Ref 14, a modification of the array along with reassignment of the particular columns was carried out. The respective factors' levels according to the adapted

Table 2 One-at-a-time full-factorial design of experiment

Parameters	Unit	Measured range	Step	Fixed value
Net power	kW	7-15	1	15
Main gas flow (Ar)	L/min	20-50	5	50
Auxiliary gas flow (He)	L/min	10-40	5	40
Feed rate	g/min	6.1-22.9	2.8	17.3
Carrier gas flow	L/min	3-7	0.5	6
Spray distance	mm	70-150	12.5	100

"Fixed value" was used for the measurements of influences of the five remaining parameters. Actual feed rate was calculated from an additional powder-collecting experiment under various revolutions of the powder feeder wheel

Table 3 Taguchi design of in-flight properties measurements

Run	Net power, kW	Main gas flow, L/min	Auxiliary gas flow, L/min	Feed rate, g/min	Carrier gas flow, L/min	Spray distance, mm	Measured	
							temperature, K	velocity, m/s
1	7	20	10	11.7	3	75	2727	151
2	7	34	24	17.3	5	100	2277	141
3	7	48	38	22.9	7	125	2125	137
4	11	20	10	17.3	5	125	2600	146
5	11	34	24	22.9	7	75	2444	174
6	11	48	38	11.7	3	100	2388	196
7	15	20	24	22.9	3	100	2617	159
8	15	34	38	11.7	5	125	2449	193
9	15	48	10	17.3	7	75	2592	193
10	7	20	38	17.3	7	100	2267	134
11	7	34	10	22.9	3	125	2212	127
12	7	48	24	11.7	5	75	2373	176
13	11	20	24	11.7	7	125	2381	150
14	11	34	38	17.3	3	75	2830	201
15	11	48	10	22.9	5	100	2344	173
16	15	20	38	22.9	5	75	2593	176
17	15	34	10	11.7	7	100	2560	174
18	15	48	24	17.3	3	125	2362	194

array could be seen from Table 3. The measurements were carried out in random order to increase the results' reliability.

The results obtained according to Taguchi design were then processed using the ANOVA (analysis of variance) statistical procedure. In ANOVA, the credibility of the measured datasets was determined by a juxtaposition of variations in the measured dataset (i.e., at different factor levels) and the overall data variations. Further to that, the corresponding parameter influences on the measured in-flight characteristics were specified and the percent contribution of every factor to the overall changes at the preselected ranges was quantified using the tool. The determined percentage distribution provides an overview on the process of plasma deposition and aids to clarify the way the powder particles are influenced in the plasma jet.

3. Results and Discussion

The combined results obtained from the full-factorial and Taguchi designs confirmed the idea of a significant effect of the system setting on the properties of the generated plasma jet and, subsequently, on the in-flight properties the TiO_2 particles attain prior to their impact on prepared substrates.

It was found that the surface temperature of the particles could vary between 2121 and 2830 K, a difference of 33%. The temperatures therefore mostly exceeded the melting point of TiO_2 (2143 K at 0.1 MPa (Ref 15)). A notable variation of up to 91% was recorded for the velocities to which the particles are propelled (a range of 127-243 m/s). The previous study of similar-sized hydroxyapatite particles (29-51 μm) (Ref 12) reported higher in-flight velocities (a range of 152-291 m/s). The ~20% difference could be caused by two factors: the difference in the actual powders' densities (incl. porosity levels) resulting in different particle weights (a difference of 21% for a typical 40-μm particle) and, therefore, different momentum transfers without regard to the volume of the particles. The second prospective factor could be the different morphologies of the individual particles (spherical hydroxyapatite versus angular TiO_2), in accordance with the study by Fukanuma et al. (Ref 16) (for a similar level of material feeding of ~20 g/min; however, it has to be reflected that the study (Ref 16) presents results of a supersonic flow in a cold spray process. For plasma spray of YSZ particles presented in Ref 17, no significant changes due to morphology were observed).

The measurement using the full-factorial design confirmed the idea of a prominent influence of net power and spray distance factors on the in-flight temperature and velocity of the TiO_2 particles. Graphical representation of the two respective factors' influences is illustrated in Fig. 3.

With an increase of 1 kW in gun net power, an increase of 39.6 K and 8.4 m/s was recorded. Such an increase in both characteristics is in accordance with the measurements by Planche et al. (Ref 18) where an increase in the net power from 20 to 40 kW increased temperatures and velocities of Al_2O_3-13 wt.% TiO_2 particles of 22-45 μm sizes from 230-310 m/s and 2400-2600 K, respectively. Further to that, the absolute values measured at a spray distance of 125 mm and a flow of $Ar + H_2$ gases of 40 and 14 L/min in Ref 18 (Sulzer Metco torch) are in good accordance with the presented study considering the increased values of net power. Using the water-stabilized plasma torch, Ctibor and Hrabovsky (Ref 19) reported insignificant changes in measured in-flight temperatures of TiO_2 particles when increasing the net power from 100 to 150 kW. The corresponding increase in velocities was measured as 43-51 m/s. The apparent difference as compared to the presented study could be caused by the notably different gun powers, particle sizes (63-125 μm),

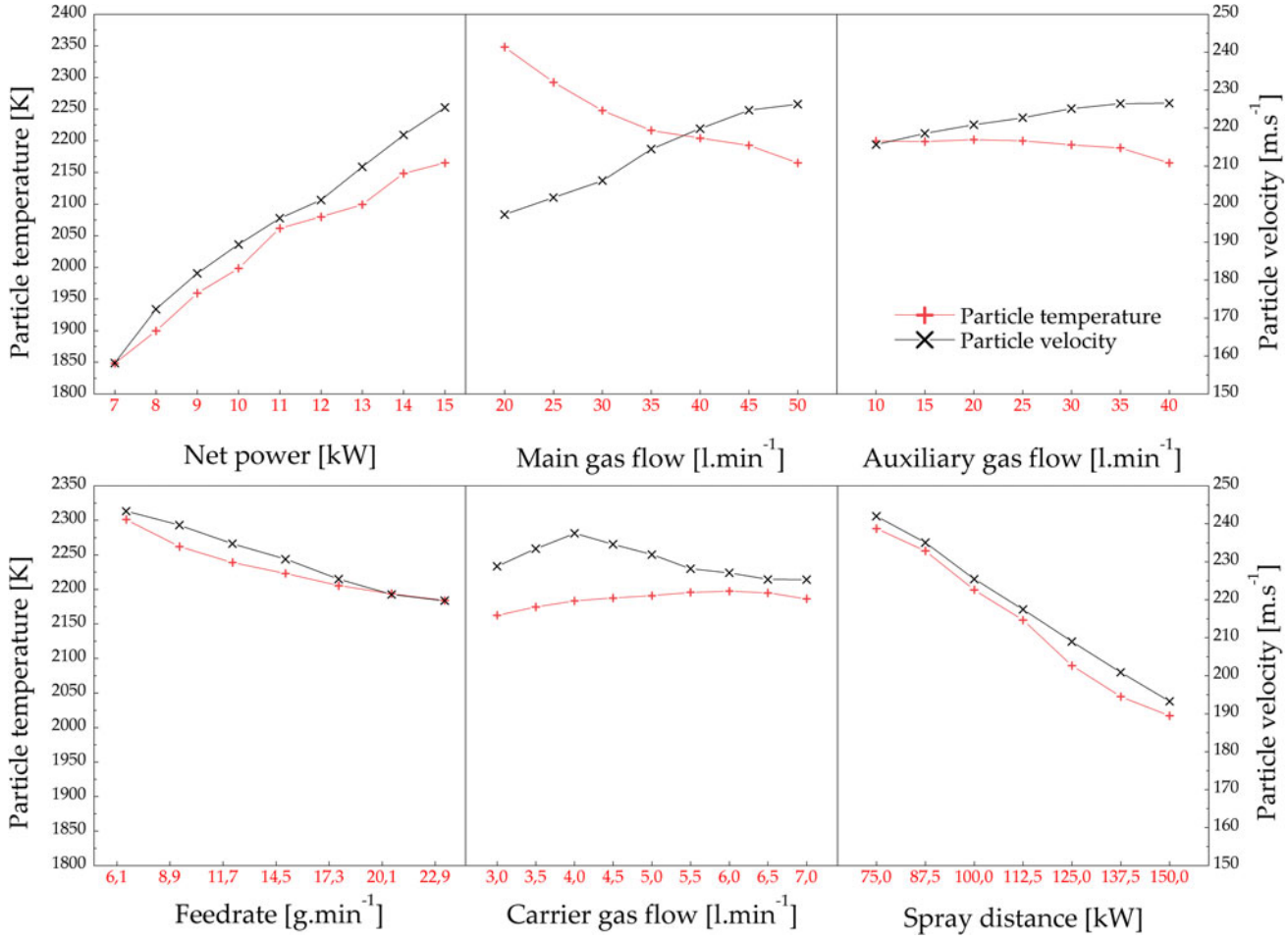

Fig. 3 In-flight temperature and velocity of TiO_2 particles measured according to one-at-a-time design of experiment

and spray distance (400 mm) used in Ref 19. Due to the spatial distribution of thermal and velocity fields in front of the gun, an increase in the spray distance of 10 mm caused a linear drop in temperature of 36 K and in velocity of 6.5 m/s. Considering the ranges of both parameters (7-15 kW for net power, 75-125 mm for spray distance), it could be concluded that the most influential factor with respect to temperature is spray distance, while net power is the most impacting factor with respect to the in-flight velocity.

Observation of the influence of carrier gas factor showed negligible changes in the measured characteristics. It could therefore be assumed that the internal powder feeding design of the SG-100 gun prevents the existence of "carrier gas effect," i.e., significant differences in the in-flight properties due to dissimilar trajectories of the particles within the plasma plume (penetration into the jet or traveling at the jet periphery) (Ref 20, 21). A direct proportion was discovered for the in-flight velocity of particles and the flow of the main arc gas (Ar). Such velocity increase resulted in shorter dwelling times in the jet and, as a consequence, lower temperatures transferred to the particles (Fig. 3). The observations are in accordance with the concept of a momentum transfer by the relatively heavy Ar ions as demonstrated, e.g., by Fang et al. (Ref 22) for ZrO_2 material. A flow of auxiliary gas (He, H_2) in general acts as an enthalpy-transferring gas without a significant increase in velocities of particles (e.g., Ref 22) (converse study on velocity increase published, e.g., in Ref 23). In accordance with the predictions, a minor increase in velocity was recorded with increasing flow of the auxiliary gas (Fig. 3). However, no incidence of the He gas flow on the in-flight temperature was recorded, in direct contrast to the predictions and reported observations (Ref 22, 23). The discovered invariance of the measured temperatures with respect to the auxiliary gas flow could probably consist in a lower enthalpy of the used gas (He versus H_2) and a subsequent reduced heat transfer to the individual particles. A significant influence of the feed rate factor was observed: A decrease of 7.1 K and 1.4 m/s was recorded for every additional 1 g/min of the powder entering the plasma jet. Such a decrease could be caused by the fact that the thermal and momentum input from the jet is transferred to a greater volume of material (~number of particles; a difference of 16.8 g/min caused a drop of 117 K and 23 m/s).

The measurements according to the Taguchi design of experiments supplement the full-factorial results. The

individual combinations of the in-flight temperatures and velocities of the particles under various combinations of the six system parameters could be seen from Fig. 4 including the measured standard deviation ranges.

The ANOVA statistical tool provided a thorough examination of the results obtained according to the Taguchi design. It allowed determination of the investigated parameters' impact strength considering their mutual interactions. The respective system parameters' influences could be seen from Fig. 5.

It was found that the most significant factors with respect to the surface temperatures of the particles are spray distance (36%), gun net power (26%), and the flow of main argon gas (16%). Such an observation is in correlation with the quantified OAAT results. The prominence of the spray distance factor is probably a consequence of the steep spatial gradient of the thermal field distribution in front of the gun as presented, e.g., by Vardelle et al. in Ref 20. With respect to the in-flight velocity of the particles during their flight, net power (48%) is the most dominant factor. The mechanism of particles' propelling via the increase in the gun net power (also observed by, e.g., Kucuk et al. in Ref 24 and Guessasma et al. in Ref 23) is not fully understood at the moment and could probably reside in the increased ionization of the momentum-transferring argon atoms (as also suggested in Ref 22). Further to the net power, the velocity of particles is directly influenced by the flow of argon arc gas (21%). The influence of spray distance factor on the velocity of the particles was specified as 14%. This fact would suggest that the attained velocity of the particles "provided" by the net power and main gas flow factors is not significantly negated by the spray distance, and the particles' impact velocities are consistent at a wide range of distances. It should be noted that the percentage contribution of the system parameters was calculated for arbitrary ranges and its validity is therefore limited within the selected bounds.

Some differences in the results provided by the two experimental approaches indicated a potential existence of the parameters' interactions. Combining the ANOVA method and the detected differences, the interactions were qualitatively determined. A medium-intense interaction was detected between the flow of the main gas and the two factors associated with the powder feeding: carrier gas flow and powder feed rate. Such an interaction could be explained by the necessity of retaining the inserted powder trajectory in the middle of the plasma jet. The geometrical condition is met when the amount of the inserted powder, the respective perpendicular component of the velocity vector (carrier gas), and the dominant flow of the main gas in the axial direction are adjusted. A weaker interaction was detected between the two powder-associated parameters and the flow of auxiliary gas, most likely due to identical causes. No interaction was detected between spray distance factor and any other investigated parameters. The influence of the distance factor could therefore be considered independent of the system settings. A similar linear effect of spray distance on the velocity and temperature of particles was observed, e.g., in Ref 25 for 8 wt.%-YSZ 45-75 μm powder. Given the non-interaction of the distance factor, the surface temperature and velocity of the TiO_2 particles could be derived as

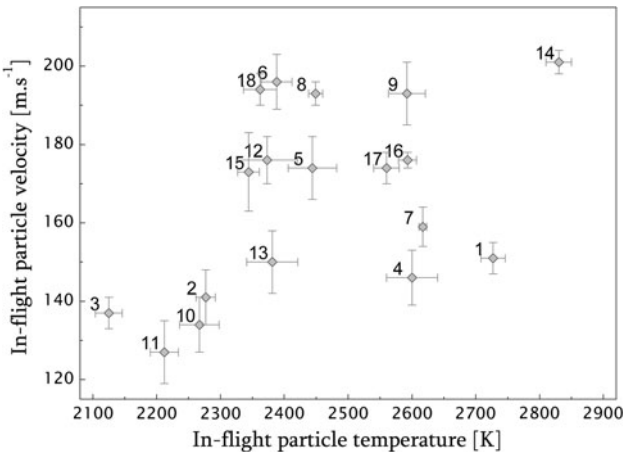

Fig. 4 In-flight temperature and velocity of TiO_2 particles measured according to Taguchi design of experiment

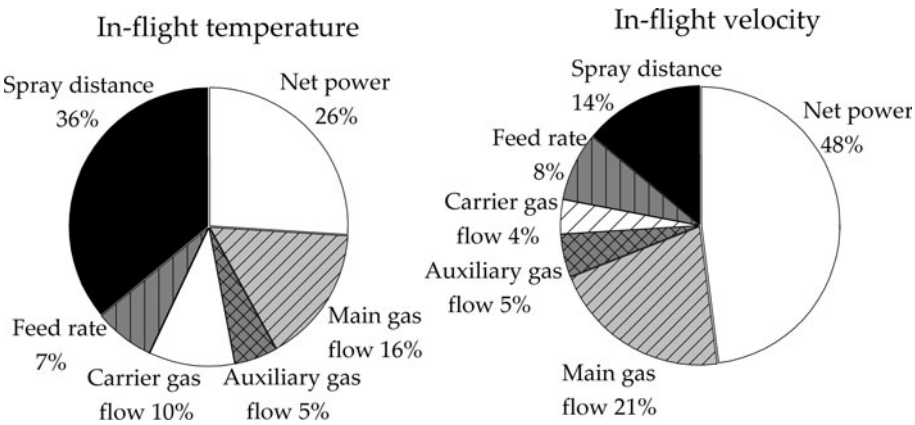

Fig. 5 Relative impact of the selected system parameters on the in-flight properties of TiO_2 particles

$$T_{TiO_2} = 2559 - 3.61 \times \text{dist} \quad (\text{K})$$
$$v_{TiO_2} = 291 - 0.65 \times \text{dist} \quad (\text{m/s})$$

where ''dist'' is the actual distance from the plasma gun orifice in mm.

4. Conclusions

The in-flight characteristics of TiO_2 rutile powder particles were studied under different plasma jet conditions influenced by the system settings. Six factors were selected to represent the versatility of the plasma system, and their respective influences on the surface temperature and velocity of the particles in-situ were studied according to basic full-factorial and advanced Taguchi designs. From the results, the following conclusions could be made:

1. Selected heat treatment (240 min at 1270 K) of the TiO_2 32-45 μm feedstock is sufficient for a full transformation of anatase $\rightarrow$ rutile phase.
2. The in-flight velocity of the particles could be varied by as much as 91%, while the surface temperature of the particles could be altered between 2121 and 2830 K (33% variation; exceeding the melting point of TiO_2) by the system settings with both characteristics substantially influencing the prospective deposited coating properties.
3. The in-flight velocity is predominantly influenced by the gun net power factor (48% relative weight) with an increase of 8.4 m/s per 1 kW of net power.
4. The in-flight (surface) temperature of the particles is significantly influenced by the spray distance factor (36% relative weight); with an increase of 10 mm in the distance, the temperature of TiO_2 particles dropped by 36 K.
5. The amount of powder entering the jet has an effect on both measured in-flight characteristics; for an additional 1 g/min of the powder feed, a drop of 7.1 K and 1.4 m/s was observed.
6. Internal feeding of the powder into the gun (SG-100 model) prevents a formation of the ''carrier gas'' phenomenon.
7. The flow of main gas (Ar) and the factors associated with powder feeding (carrier gas, feed rate) are interconnected and their respective values need to be correlated to retain optimum in-jet trajectories due to the interaction.
8. Spray distance is an independent factor and its incidence on the measured in-flight properties is retained regardless the plasma system settings.

Acknowledgments

The Project has been funded from the SoMoPro programme. Research leading to these results has received a financial contribution from the European Community within the Seventh Framework Programme (FP/2007-2013) under Grant Agreement No. 229603. The research is also co-financed by the South Moravian Region. The EC OP Project No. CZ.1.07./2.3.00/20.0197 is gratefully acknowledged.

References

1. L.L. Hench, Bioceramics—from Concept to Clinic, *J. Am. Ceram. Soc.*, 1991, **74**(7), p 1487-1510
2. C. Larsson, P. Thomsen, J. Lausmaa, M. Rodahl, B. Kasemo, and L.E. Ericson, Bone Response to Surface Modified Titanium Implants: Studies on Electropolished Implants with Different Oxide Thicknesses and Morphology, *Biomaterials*, 1994, **15**(13), p 1062-1074
3. N. Huang, Y.R. Chen, J.M. Luo, J. Yi, R. Lu, J. Xiao, Z.N. Xue, and X.H. Liu, In Vitro Investigation of Blood Compatibility of Ti with Oxide Layers of Rutile Structure, *J. Biomater. Appl.*, 1994, **8**(4), p 404-412
4. V. Sollazzo, F. Pezzetti, A. Scarano, A. Piattelli, L. Massari, G. Brunelli, and F. Carinci, Anatase Coating Improves Implant Osseointegration In Vivo, *J. Craniofac. Surg.*, 2007, **18**(4), p 806-810
5. I. Tsyganov, M.F. Maitz, E. Wieser, F. Prokert, E. Richter, and A. Rogozin, Structure and Properties of Titanium Oxide Layers Prepared by Metal Plasma Immersion Ion Implantation and Deposition, *Surf. Coat. Technol.*, 2003, **174-175**, p 591-596
6. H.K. Tsou, P.Y. Hsieh, M.H. Chi, C.J. Chung, and J.L. He, Improved Osteoblast Compatibility of Medical-Grade Polyetheretherketone Using Arc Ionplated Rutile/Anatase Titanium Dioxide Films for Spinal Implants, *J. Biomed. Mater. Res. A*, 2012, **100A**(10), p 2787-2792
7. S. Forberg, Ceramic Containers for Spent Nuclear Fuel: On the Corrosion Resistance of Rutile, *Adv. Ceramics*, 1986, **20**, p 321-327
8. I. Tsyganov, M.F. Maitz, and E. Wieser, Blood Compatibility of Titanium-Based Coatings Prepared by Metal Plasma Immersion Ion Implantation, Deposition, *Appl. Surf. Sci.*, 2004, **235**(1-2), p 156-163
9. P. Fauchais, Understanding Plasma Spraying, *J. Phys. D*, 2004, **37**(9), p R86-R108
10. P. Fauchais, M. Fukumoto, A. Vardelle, and M. Vardelle, Knowledge Concerning Splay Formation: An Invited Review, *J. Therm. Spray. Technol.*, 2004, **13**(3), p 337-360
11. P.I. Gouma and M.J. Mills, Anatase-to-Rutile Transformation in powders, *J. Am. Ceram. Soc.*, 2001, **84**(3), p 619-622
12. J. Cizek and K.A. Khor, Role of In-Flight Temperature, Velocity of Powder Particles on Plasma Sprayed Hydroxyapatite Coating Characteristics, *Surf. Coat. Technol.*, 2012, **206**(8-9), p 2181-2191
13. D.D. Frey, A Role for ''One-Factor-at-a-Time'' Experimentation in Parameter Design, *Res. Eng. Des.*, 2003, **14**(3), p 65-74
14. G. Taguchi, *Quality Engineering in Production Systems*, McGraw-Hill, New York, 1988
15. Y. Li and T. Ishigaki, Thermodynamic Analysis of Nucleation of Anatase, Rutile from TiO_2 Melt, *J. Cryst. Growth*, 2002, **242**(3-4), p 511-516
16. H. Fukanuma, N. Ohno, B. Sun, and R. Huang, In-Flight Particle Velocity Measurements with DPV-2000 in Cold Spray, *Surf. Coat. Technol.*, 2006, **201**(5), p 1935-1941
17. V. Srinivasan, *A Critical Assessment of In-Flight Particle State During Plasma Spraying of YSZ, Its Implications on Coating Properties, Process Reliability*, Stony Brook University, Stony Brook, NY, 2007
18. M.P. Planche, B. Normand, E. Suzon, and C. Coddet, The Relationships Between In-Flight Particles Characteristics, Coatings Properties Under Plasma Spraying Conditions, *Thermal Spray 2001: New Surfaces for a New Millenium*, ASM International, Materials Park, OH, 2001, p 771-777
19. P. Ctibor and M. Hrabovsky, Plasma Sprayed TiO_2: The Influence of Power of an Electric Supply on Particle Parameters in the Flight, Character of Sprayed Coating, *J. Eur. Ceram. Soc.*, 2010, **30**(15), p 3131-3136

20. M. Vardelle, A. Vardelle, and P. Fauchais, Spray Parameters, Particle Behavior Relationships During Plasma Spraying, *J. Therm. Spray. Technol.*, 1993, **2**(1), p 79-91
21. K. Neufuss, J. Ilavsky, B. Kolman, J. Dubsky, P. Rohan, and P. Chraska, Variation of Plasma Spray Deposits Microstructure, Properties Formed by Particles Passing through Different Areas of Plasma Jet, *Ceram.-Silikaty*, 2001, **45**(1), p 1-8
22. J.C. Fang, W.J. Xu, Z.Y. Zhao, and H.P. Zheng, In-Flight Behaviors of ZrO_2 Particle in Plasma Spraying, *Surf. Coat. Technol.*, 2007, **201**(9-11), p 5671-5675
23. S. Guessasma, G. Montavon, and C. Coddet, Velocity, Temperature Distributions of Alumina-Titania In-Flight Particles in the Atmospheric Plasma Spray Process, *Surf. Coat. Technol.*, 2005, **192**(1), p 70-76
24. A. Kucuk, R.S. Lima, and C.C. Berndt, Influence of Plasma Spray Parameters on In-Flight Characteristics of ZrO_2-8 wt.% Y_2O_3 Ceramic Particles, *J. Am. Ceram. Soc.*, 2001, **84**(4), p 685-692
25. Z. Salhi, S. Guessasma, and N. Fenineche, Yttria-Stabilized Zirconia In-Flight Particle Characteristics Under Vacuum Plasma Spray Conditions, *Vacuum*, 2009, **83**(11), p 1382-1387